Tight-binding study of anomalous Hall effect in ferromagnetic 3*d* transition metals

T. Naito, D. S. Hirashima, and H. Kontani
Department of Physics, Nagoya University, Nagoya 464-8602, Japan
(Received 6 November 2009; revised manuscript received 24 February 2010; published 12 May 2010)

Anomalous Hall conductivity in ferromagnetic 3*d* transition metals is calculated using realistic tight-binding models assuming the intrinsic origin of the effect. The order of magnitude and sign of the obtained results are found to agree with experimental and previous theoretical results, supporting the intrinsic origin of the anomalous Hall effect in ferromagnetic 3*d* transition metals. Furthermore, it is shown that magnitude and sign of the anomalous Hall conductivity can be explained as a consequence of the dependence of the Hall conductivity on electron number found in our previous study.

DOI: 10.1103/PhysRevB.81.195111 PACS number(s): 72.15.Gd, 71.20.Be, 75.47.−m

I. INTRODUCTION

A magnetic field B deflects carriers of current j in a normal metal through the Lorentz force. If B is perpendicular to j, a finite electric field E is generated in the direction perpendicular to both B and j. The Hall resistivity $\rho_H=E/j$ is proportional to B and the coefficient $R_H=\rho_H/B$ is called the Hall coefficient. In a ferromagnetic metal, additional term proportional to the magnetization M appears in ρ_H and the Hall resistivity is conventionally expressed as $\rho_H=R_HB+4\pi MR_H^a$. The coefficient R_H^a is called the anomalous Hall coefficient. Usually, R_H^a is much larger than R_H, $\rho_H\simeq 4\pi MR_H^a=\rho_H'$.

Mechanism of the anomalous Hall effect (AHE) has been a well studied, yet controversial subject. It was Karplus and Luttinger[1] (KL) that first explained the AHE as a result of spin-orbit interaction (SOI). They found the anomalous Hall conductivity (AHC) σ_{xy}^a that is independent of resistivity ρ, i.e., independent of impurity concentration ($\rho_H'\propto\rho^2$). That is why the AHE they discussed is called the intrinsic AHE. Although notion that spin-orbit interaction is the principal cause of the AHE was readily accepted, the intrinsic mechanism itself was not. Soon after KL, Smit[2] proposed an extrinsic mechanism, skew scattering mechanism, for the AHE. In the presence of spin-orbit interaction, conduction electrons are scattered by impurities asymmetrically depending on the direction of spin (skew scattering), which, Smit argued, results in the AHE. In contrast to the intrinsic AHC, the AHC caused by skew scattering is proportional to $\rho^{-1}(\rho_H'\propto\rho)$. Furthermore, Berger suggested another extrinsic mechanism, side-jump mechanism, which predicts $\sigma_{xy}^a\propto\mathcal{O}(\rho^0)$.[3]

In spite of much effort, the interpretation of the AHE has been controversial so far. It appears that extrinsic mechanism has been more widely accepted than the intrinsic mechanism. One of the reasons must be that there have been no precise calculations of the AHE until recently. However, the AHC in various materials has now been calculated based on the intrinsic mechanism using tight-binding models[4–6] and the first-principles calculations.[7–10] The order of magnitude and sign of the results agree with experimental findings, thus giving much credibility to the intrinsic mechanism of the AHE.

The purpose of this work is to study the intrinsic AHE in ferromagnetic 3*d* transition metals (Fe, Co, and Ni) using realistic tight-binding models, to investigate the mechanism of the AHE in detail, and give a semiquantitative understanding of the AHE and the spin-Hall effect (SHE), which is an analog of the AHE in normal metals (or semiconductors),[11,12] in a unified way.

In previous studies,[7–10] the AHC is expressed as an integral of the Berry curvature over the Brillouin zone.[13,14] The expression is identical to that obtained by KL. However, using the linear-response theory, it was found that additional terms appear in the expression of the AHC.[15,16] In this work, we calculate the AHC taking account of all the terms, and find that the most appropriate expression for the AHC in a wide range of damping rate is not the Berry curvature term, but another term, the Fermi-surface term.

For the actual calculations of the AHC, we use the Naval Research Laboratory tight-binding (NRL-TB) model.[17,18] We add atomic spin-orbit interaction to it to describe the AHE. The use of tight-binding models enables us to calculate the AHC more easily with a fine mesh of the Brillouin zone, compared with calculations with a direct use of first-principles calculations.[19] Furthermore, we can analyze the mechanism of the AHE in detail; for example, we can calculate contributions to the AHE from different orbitals separately.

Along with the AHE, the SHE has now attracted much interest. The SHE is an analog of the AHE in paramagnetic metals.[11,12] As the numbers of electrons of different spin polarization are equal in paramagnets, there occurs no net charge current, but net spin current can be induced by an electric field in the presence of SOI. This is the SHE. At first, the SHE was observed in semiconductors[20,21] and Al,[22] but later a large SHE was observed in a transition metal, Pt.[23,24] It is clear that SOI is also essential for the spin-Hall conductivity (SHC), but similarly to the case with the AHE, there have been controversies over the mechanism of the SHE (intrinsic or extrinsic) since the intrinsic origin of the SHE was put forward by Murakami *et al.*[25] and Sinova *et al.*[26] For transition metals and compounds, quantitatively reliable calculations based on the intrinsic mechanism have now been carried out,[27–29] as in the case with the AHC. Indeed, we have systematically calculated the SHC in 4*d* and 5*d* transition metals using the NRL-TB model,[30] and obtained the SHC in Pt that is in semiquantitative agreement with the experimental results.[29,30] Furthermore, we discussed the systematic change in sign of the SHC between light transition

metals and heavy transition metals;[31] the SHC is negative for lighter ones and positive for heavier ones. This change in sign of the SHC has indeed been partially confirmed experimentally.[32] We have also succeeded in explaining this trend and estimating the magnitude of the SHC; the essence of the effect is indeed the orbital Hall effect and orbital Hall conductivity is always positive. The sign of the SHC is determined by the sign of the coupling $\langle \boldsymbol{s}\cdot\boldsymbol{\ell}\rangle$.[31] It was also pointed out that the SHC is caused by the effective Aharonov-Bohm magnetic flux induced by combination of SOI and orbital-dependent electron transfers.[27,30] In this study, we apply the same idea and the method to 3*d* ferromagnetic transition metals to study the AHE. In doing so, we can understand the AHE and SHE on the same basis and give a semiquantitative interpretation of the AHE in 3*d* ferromagnetic metals.

In the next section, models and the method of calculations are explained, and in Sec. III numerical results are shown. In Sec. IV, we give an analysis of the present results as compared with the SHE in transition metals and show that the AHC in the 3*d* ferromagnetic metals can be semiquantitatively understood. Final section is devoted to summary and discussion. In the text, we mainly study the AHE in Co and Ni, and show results for Fe obtained with a different tight-binding parameter set in the Appendix.

II. THEORY

To describe the electronic states of transition metals, we use the NRL-TB model. In the NRL-TB model, 3*d*, 4*s*, and 4*p* electrons are considered in describing electronic states in 3*d* transition metals and a parameter set for the ferromagnetic state is given in addition to that for the paramagnetic state for Fe, Ni, and Co. We use those parameter sets for the ferromagnetic states. We then introduce the SOI. We consider the atomic SOI for only *d* electrons. Then, the Hamiltonian is given

$$\hat{\mathcal{H}} = \begin{pmatrix} \hat{\mathcal{H}}_{0\uparrow} + \lambda\hat{\ell}_z/2 & \lambda(\hat{\ell}_x - i\hat{\ell}_y)/2 \\ \lambda(\hat{\ell}_x + i\hat{\ell}_y)/2 & \hat{\mathcal{H}}_{0\downarrow} - \lambda\hat{\ell}_z/2 \end{pmatrix}, \tag{1}$$

where $\mathcal{H}_{0\sigma}$ is a $9\times 9(18\times 18)$ matrix defined by a parameter set in the NRL-TB model for bcc and fcc (hcp) structures. We understand the SOI in Eq. (1) works only for *d* electrons [matrices ℓ_μ are 5×5 (or 10×10) ones]. For the spin-orbit coupling λ, we use the Herman-Skillman parameters[33] (see Table I).

Originally, the NRL-TB Hamiltonian is expressed with nonorthogonal bases,

$$\hat{\mathcal{H}} = \sum_{\boldsymbol{k}} \sum_{\alpha,\beta} c^\dagger_{\boldsymbol{k}\alpha} h_{\alpha\beta}(\boldsymbol{k}) c_{\boldsymbol{k}\beta}, \tag{2}$$

where $c_{\boldsymbol{k}\alpha}$ is the annihilation operator of an electron with momentum $\boldsymbol{k}$ in a spin-orbital state α. These operators do not satisfy the canonical anticommutation relations, but

TABLE I. Crystal structure and the spin-orbit interaction constant λ for 3*d* transition metals (Ref. 33).

Element	Structure	SOI (mRy)
Sc	hcp	0.9
Ti	hcp	1.8
V	bcc	2.32
Cr	bcc	2.84
Mn	bcc	4.07
Fe	bcc	5.30
Co	hcp	6.72
Ni	fcc	8.14
Cu	fcc	10.00

$$\{c_{\boldsymbol{k}\alpha}, c^\dagger_{\boldsymbol{k}'\beta}\} = \delta_{\boldsymbol{k},\boldsymbol{k}'} O^{-1}_{\alpha\beta}(\boldsymbol{k}), \tag{3}$$

where $\hat{O}(\boldsymbol{k})$ is a Fourier transform of the overlap integral matrix. We can transform the Hamiltonian into a form expressed by orthonormal bases,

$$\hat{\mathcal{H}} = \sum_{\boldsymbol{k}} \sum_{\alpha,\beta} \bar{c}^\dagger_{\boldsymbol{k}\alpha} \bar{h}_{\alpha\beta}(\boldsymbol{k}) \bar{c}_{\boldsymbol{k}\beta}, \tag{4}$$

where

$$\{\bar{c}_{\boldsymbol{k}\alpha}, \bar{c}^\dagger_{\boldsymbol{k}'\beta}\} = \delta_{\boldsymbol{k},\boldsymbol{k}'}\delta_{\alpha\beta}. \tag{5}$$

The retarded and advanced Green's functions defined by $(\bar{c}_{\boldsymbol{k}\alpha}, \bar{c}^\dagger_{\boldsymbol{k}\beta})$ is then expressed as

$$\hat{G}^{\mathrm{R,A}}(\boldsymbol{k},\omega) = (\omega + \mu - \hat{\bar{h}} \pm i\hat{\Gamma})^{-1}, \tag{6}$$

where the sign + (−) is for the retarded (advanced) one and the damping rate $\hat{\Gamma}$ is also added. For local potential scattering (and in the absence of SOI), $\hat{\Gamma}$ is diagonal when expressed with orbital bases. In the Born approximation, each element is proportional to the density of states of each orbital. In transition metals, the density of states of each orbital is not very different for *d* orbital, and we put the damping rate to be constant; $\hat{\Gamma} = \gamma\hat{E}$, where $\hat{E}$ is a unit matrix.[34] Then, the Green's function are diagonalized (with a unitary matrix $\hat{U}$) as

$$[(\hat{U}^\dagger(\boldsymbol{k})\hat{G}^{\mathrm{R,A}}(\boldsymbol{k},\omega)\hat{U}(\boldsymbol{k})]_{nn'} = \frac{\delta_{nn'}}{\omega - E_n(\boldsymbol{k}) \pm i\gamma}. \tag{7}$$

Charge current-density operator $\hat{j}_\mu$ is defined by[30]

$$\hat{j}_\mu(\boldsymbol{k}) = -e\frac{\partial\hat{h}(\boldsymbol{k})}{\partial k_\mu} + \delta\hat{j}_\mu(\boldsymbol{k}), \tag{8}$$

where $\delta\hat{j}$ originates from nonorthogonality of bases and is given by

$$\delta\hat{j}_\mu = \frac{1}{2}[\hat{h}(\boldsymbol{k})\hat{D}_\mu(\boldsymbol{k}) + \hat{D}_\mu(\boldsymbol{k})\hat{h}(\boldsymbol{k})] \tag{9}$$

with

$$\hat{D}_\mu(\boldsymbol{k}) = \left[\frac{\partial}{\partial k_\mu}\hat{O}^{-1}(\boldsymbol{k})\right]\hat{O}(\boldsymbol{k}). \tag{10}$$

$\delta\hat{j}$ contributes only modestly ($\lesssim 10\%$) to conductivities.

Now that the current-density operators are defined, it is rather straightforward to calculate Hall conductivity σ_{xy} following the linear-response theory,[15]

$$\sigma_{xy} = \sigma_{xy}^{\mathrm{I}} + \sigma_{xy}^{\mathrm{II}}, \tag{11}$$

where

$$\sigma_{xy}^{\mathrm{I}} = \frac{1}{2\pi N}\sum_{\boldsymbol{k}} \mathrm{Tr}[\hat{j}_x\hat{G}^{\mathrm{R}}\hat{j}_y\hat{G}^{\mathrm{A}}]|_{\omega=0} \tag{12}$$

and

$$\sigma_{xy}^{\mathrm{II}} = -\frac{1}{4\pi N}\sum_{\boldsymbol{k}}\int_{-\infty}^{0} d\omega\, \mathrm{Tr}\{[\hat{j}_x(\hat{G}^{\mathrm{R}})'\hat{j}_y\hat{G}^{\mathrm{R}} - \hat{j}_x\hat{G}^{\mathrm{R}}\hat{j}_y(\hat{G}^{\mathrm{R}})'] - (R\to A)\}, \tag{13}$$

where $(\hat{G}^\nu)' = \partial\hat{G}^\nu/\partial\omega$ and the case with $T=0$ is considered. As we consider only the AHC in this study, we drop the suffix a for σ_{xy} from now. The first term σ_{xy}^{I} has contributions only from the Fermi surface and is called the Fermi-surface term. Its explicit expression is given by

$$\sigma_{xy}^{\mathrm{I}} = -\frac{1}{2\pi N}\sum_{\boldsymbol{k}}\sum_{n\neq n'} \mathrm{Im}[(\tilde{j}_x)_{n'n}(\tilde{j}_y)_{nn'}] \times \mathrm{Im}\left\{\frac{1}{[E_n(\boldsymbol{k}) - i\gamma][E_{n'}(\boldsymbol{k}) + i\gamma]}\right\}, \tag{14}$$

where $(\tilde{j}_\mu)_{nn'} = [\hat{U}^\dagger(\boldsymbol{k})\hat{j}_\mu(\boldsymbol{k})\hat{U}(\boldsymbol{k})]_{nn'}$.

The second term $\sigma_{xy}^{\mathrm{II}}$ is represented as integral over the occupied states and is called the Fermi sea term. After a little algebra, we can rewrite $\sigma_{xy}^{\mathrm{II}}$ as

$$\sigma_{xy}^{\mathrm{II}} = \sigma_{xy}^{\mathrm{II}a} + \sigma_{xy}^{\mathrm{II}b}, \tag{15}$$

where

$$\sigma_{xy}^{\mathrm{II}a} = -\frac{1}{2\pi N}\sum_{\boldsymbol{k}}\sum_{n\neq n'} \frac{\mathrm{Im}[(\tilde{j}_x)_{n'n}(\tilde{j}_y)_{nn'}]}{E_n(\boldsymbol{k}) - E_{n'}(\boldsymbol{k})} \times \mathrm{Im}\left\{\frac{E_n(\boldsymbol{k}) + E_{n'}(\boldsymbol{k}) - 2i\gamma}{[E_n(\boldsymbol{k}) - i\gamma][E_{n'}(\boldsymbol{k}) - i\gamma]}\right\} \tag{16}$$

and

$$\sigma_{xy}^{\mathrm{II}b} = \frac{1}{\pi N}\sum_{\boldsymbol{k}}\sum_{n\neq n'} \frac{\mathrm{Im}[(\tilde{j}_x)_{n'n}(\tilde{j}_y)_{nn'}]}{[E_n(\boldsymbol{k}) - E_{n'}(\boldsymbol{k})]^2} \times \mathrm{Im}\left\{\ln\left[\frac{E_n(\boldsymbol{k}) - i\gamma}{E_{n'}(\boldsymbol{k}) - i\gamma}\right]\right\}. \tag{17}$$

As $\gamma\to 0$, $\sigma_{xy}^{\mathrm{II}b}$ is rewritten as

$$\sigma_{xy}^{\mathrm{II}b} = \frac{1}{N}\sum_{\boldsymbol{k}} f[E_n(\boldsymbol{k})]\Omega_n(\boldsymbol{k}), \tag{18}$$

where $\Omega_n(\boldsymbol{k})$ represents the Berry curvature defined by

$$\Omega_n(\boldsymbol{k}) = \sum_{n'(\neq n)} \frac{2\,\mathrm{Im}[(\tilde{j}_x)_{n'n}(\tilde{j}_y)_{nn'}]}{[E_n(\boldsymbol{k}) - E_{n'}(\boldsymbol{k})]^2}, \tag{19}$$

and finite temperature cases are considered. Moreover, it is straightforward to show that

$$\mathrm{Im}\left\{\frac{E_n(\boldsymbol{k}) - E_{n'}(\boldsymbol{k})}{[E_n(\boldsymbol{k}) - i\gamma][E_{n'}(\boldsymbol{k}) + i\gamma]}\right\} = -\mathrm{Im}\left\{\frac{E_n(\boldsymbol{k}) + E_{n'}(\boldsymbol{k}) - 2i\gamma}{[E_n(\boldsymbol{k}) - i\gamma][E_{n'}(\boldsymbol{k}) - i\gamma]}\right\}, \tag{20}$$

that is, $\sigma_{xy}^{\mathrm{I}} = -\sigma_{xy}^{\mathrm{II}a}$,[35] in the limit of $\gamma\to 0$. This justifies the use of the Berry curvature term $\sigma_{xy}^{\mathrm{II}b}$ to calculate the AHC *in the clean limit* under the assumption of constant γ.

For a semiconductor or an insulator, where the chemical potential is in the energy gap, $\sigma_{xy} = \sigma_{xy}^{\mathrm{II}b}$, i.e., the Hall conductivity is expressed solely with the Berry phase term, as long as the damping rate is smaller than the energy gap. It is frequently assumed that the same relation also holds in metals but the relation is not necessarily valid at $\gamma\neq 0$ even if γ=const for all the bands. In this work, we calculate Hall conductivity σ_{xy} taking all the contributions into account, $\sigma_{xy} = \sigma_{xy}^{\mathrm{I}} + \sigma_{xy}^{\mathrm{II}}$.

In general, impurity scattering contributes to conductivities not only through the self-energy correction but also through vertex correction. If only s and d electrons are concerned, the vertex correction exactly cancels for local impurity potential. In the present case, as we also consider p electrons, the vertex correction can remain finite even for local scattering potential. However, we have confirmed that the correction turns out to be also small in $3d$ transition metals as in $4d$ and $5d$ ones[30] because the density of states of p electrons are small at the Fermi surface. We neglect the vertex correction in this work.

III. RESULTS

Using the NRL-TB model, we can obtain the energy dispersions of electrons in $3d$ transition ferromagnetic metals, which agree well with previous calculations.[36,37] It is necessary to divide the Brillouin zone into a fine mesh in calculating Eqs. (12), (16), and (17) to obtain well-converged and reliable results. For Fe (bcc) and Ni (fcc), we increase the number of $\boldsymbol{k}$ points up to 512^3, and for Co (hcp) up to 256^3. Figure 1 shows the Hall conductivity σ_{xy} of Ni and Co as a function of the damping rate γ. As $\gamma\to 0$, the Hall conductivity becomes independent of γ, which is a natural consequence of the intrinsic mechanism. In this limit, the relation $\sigma_{xy}^{\mathrm{I}} + \sigma_{xy}^{\mathrm{II}b} \simeq \sigma_{xy}^{\mathrm{II}} \simeq 0$ holds. Therefore, $\sigma_{xy} \simeq \sigma_{xy}^{\mathrm{I}} \simeq \sigma_{xy}^{\mathrm{II}b}$ in the clean limit. On the other hand, as γ becomes large, $|\sigma_{xy}|$ gradually decreases, that is, the AHC due to the intrinsic mechanism also depends on the impurity concentration as the system becomes dirty. In the dirty case, the AHC is

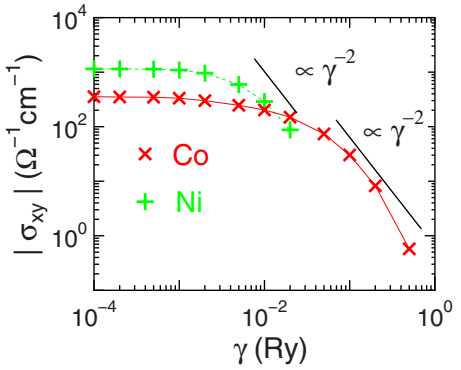

FIG. 1. (Color online) Magnitude of anomalous Hall conductivity σ_{xy} in Co and Ni as a function of damping rate γ. At $\gamma=0.001$ Ry, $\rho \simeq 10$ $\mu\Omega$ cm for Ni, and 5 $\mu\Omega$ cm for Co.

roughly proportional to γ^{-2}, $\sigma_{xy} \sim \gamma^{-2}$.[38] As is shown in Fig. 2, it is necessary to consider not only the Berry curvature term $\sigma_{xy}^{\mathrm{II}b}$, but also other contributions to describe this coherent-incoherent crossover. Actually, in the dirty case, the relation $\sigma_{xy} \simeq \sigma_{xy}^{\mathrm{I}}$ also holds. It is therefore more appropriate to estimate σ_{xy} with the Fermi-surface contribution σ_{xy}^{I} in a wider range of γ. The relation $\sigma_{xy} \simeq \sigma_{xy}^{\mathrm{II}b}$ holds only in the clean limit.

Table II summarizes the results of the AHC for ferromagnetic $3d$ transition metals. Results obtained with the maximum $\boldsymbol{k}$ points are shown here. We present the results for $\gamma=0.001$ Ry. As is shown in Fig. 1, the values of $|\sigma_{xy}|$ have almost saturated at this value of γ. The values in Table II are therefore considered to be those of the intrinsic AHC in the clean limit. For comparison, previous theoretical and experimental results are also shown. It can be seen that not only the

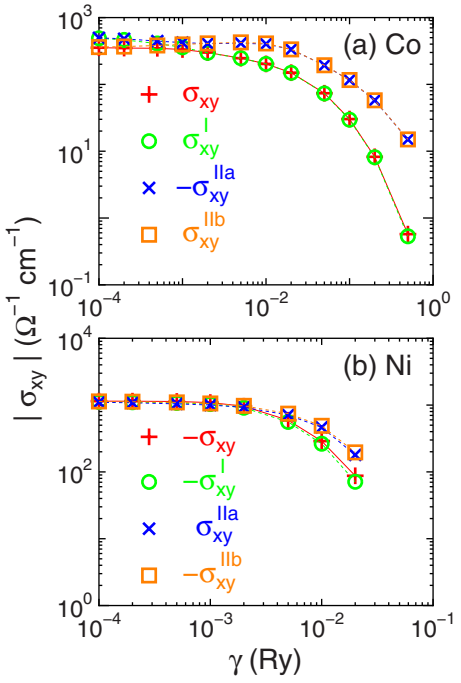

FIG. 2. (Color online) Contributions $\sigma_{xy}^{A\mu}$ ($A=\mathrm{I},\mathrm{II}$ and $\mu=a,b$) to anomalous Hall conductivity σ_{xy} in (a) Co and (b) Ni as functions of damping rate γ.

TABLE II. Anomalous Hall conductivity σ_{xy} in $3d$ ferromagnetic transition metals.

σ_{xy} [$(\Omega$ cm$)^{-1}$]	Fe	Co	Ni
Present work[a]	247	341	−1087
Ref. 8	751	492[b]	−2073[b]
Ref. 10	750	478	−2275
Experiment	1032[c]	205[d]	−646[e]

[a]At $\gamma=0.001$ Ry.
[b]Quoted in Ref. 10.
[c]Reference 39.
[d]Reference 40.
[e]Reference 41.

sign but also the order of magnitude agree with each other. Here, it should be noted that those experimental values are typical values of the AHC. Indeed, the reported values of the AHC in experimental studies scatter considerably,[39–42] although results for the order of magnitude and sign have been consistently obtained. The finding that the order of magnitude and sign of the AHC are correctly obtained in this study as in the previous studies[8–10] supports the intrinsic mechanism of the AHE in those ferromagnets.

In contrast to the cases with Co and Ni, the agreement of the result for Fe with the previous calculations is poorer. This point is discussed in the Appendix separately. In the next section, we explain the order of magnitude and the sign of the AHC in those ferromagnets based on the results obtained with the NRL-TB model. We emphasize that the obtained results can do for that purpose although the agreement with the previous ones or experimental ones are not perfect.

IV. AHC AND SHC

The SHE in a paramagnet is an analog of the AHE in a ferromagnet, and there is a close connection between the SHC σ_{xy}^{S} and the AHC σ_{xy}. Spin current density $\boldsymbol{j}^{\mathrm{S}}$ and charge current density $\boldsymbol{j}$ can be written as

$$\boldsymbol{j}^{\mathrm{S}} = \frac{\hbar}{2}(j^{\uparrow} - j^{\downarrow}) \tag{21}$$

and

$$\boldsymbol{j} = -e(j^{\uparrow} + j^{\downarrow}), \tag{22}$$

respectively, where j^{σ} is the current density of electrons of spin σ. As we have found that it is $\lambda \ell_z s_z$ that gives the dominant contribution to conductivity among the spin-orbit interaction $\lambda \boldsymbol{\ell} \cdot \boldsymbol{s}$, as in the case of the SHC in $4d$ and $5d$ transition metals,[30] we can rewrite the SHC and the AHC as

$$\frac{|e|}{\hbar}\sigma_{xy}^{\mathrm{S}} \simeq (\sigma_{xy}^{\uparrow} + \sigma_{xy}^{\downarrow}) \tag{23}$$

and

$$\sigma_{xy} \simeq -2(\sigma_{xy}^{\uparrow} - \sigma_{xy}^{\downarrow}). \tag{24}$$

Here, σ_{xy}^{σ} represents conductivity of electrons with spin σ, and its sign and numerical factor are defined for later conve-

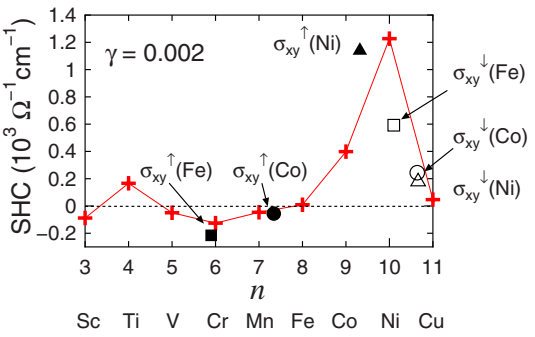

FIG. 3. (Color online) Spin-Hall conductivity $\sigma_{xy}^{S}(\times|e|/\hbar)$ of $3d$ transition metals. Damping rate γ is γ=0.002 Ry. Also plotted are $2\sigma_{xy}^{\uparrow}$ (closed symbols) and $2\sigma_{xy}^{\downarrow}$ (open symbols), which are obtained from the AHC and SHC in the ferromagnetic phase, as a function of $2n_{\sigma}$ for Fe (squares), Co (dots), and Ni (triangles). σ_{xy}^{σ}'s in Fe are obtained with the tight-binding parameter set described in the Appendix.

nience. In a paramagnet, $\sigma_{xy}^{\uparrow}=\sigma_{xy}^{\downarrow}$, and $\sigma_{xy}=0$, as is expected. Using Eqs. (23) and (24), we now argue that the AHC in the ferromagnetic $3d$ transition metals can be semiquantitatively understood.

To do so, we first discuss the dependence of σ_{xy}^{σ} on the total electron number n. We calculate the SHC σ_{xy}^{S} for $3d$ transition paramagnetic metals and the results are shown in Fig. 3 as a function of n. For Cr, Fe, Co, and Ni, a paramagnetic state is assumed here, and a simple bcc crystal structure is assumed for Mn. The dependence of $\sigma_{xy}^{S}(=2\sigma_{xy}^{\uparrow}=2\sigma_{xy}^{\downarrow})$ on n is quite similar to that found for $4d$ and $5d$ transition metals.[30] For lighter elements, σ_{xy}^{S} is negative, and it changes sign at $n\simeq 7-8$, and is positive for heavier elements.

This dependence of σ_{xy}^{S} on the electron number n was successfully explained by a simple model.[31] According to this theory, the SHC of transition metals is approximately given by

$$\sigma_{xy}^{S} \simeq \frac{\langle \ell_z s_z \rangle}{\hbar^2}\frac{|e|}{a}, \tag{25}$$

where a is the lattice constant. The average $\langle \ell_z s_z \rangle$ is proportional to the spin-orbit interaction λ (in the limit of $\lambda \to 0$), which is larger in a heavier element. Moreover, Hund's rule tells us that $\langle \ell_z s_z \rangle$ is negative for less-than-half-filled transition elements and that it is positive for more-than-half-filled ones. We thus expect that σ_{xy}^{S} is negative and rather small in its absolute magnitude for lighter transition metals, and is positive and rather large in heavier transition metals. In noble metals, where d orbitals are fully filled and the electron states near the Fermi surface mainly consists of s electrons, spin-orbit interaction plays only a minor role, and σ_{xy}^{S} must become small. Numerical results of σ_{xy}^{S} not only for $4d$ and $5d$ transition metals[30] but also for $3d$ transition metals (Fig. 3) are well explained by these arguments. Note, however, that the SHC for Ti is found to be positive, deviating the general trend of the SHC. We discuss this point in the Appendix.

In ferromagnets, $\sigma_{xy}^{\uparrow} \neq \sigma_{xy}^{\downarrow}$, because electron number of each spin direction n_{σ} differs from each other, $n_{\uparrow} \neq n_{\downarrow}$. Each σ_{xy}^{σ} must depend on n_{σ} in the same way as $\sigma_{xy}^{S}(=2\sigma_{xy}^{\sigma})$ in paramagnets does on n. This explains the sign (and the magnitude) of the AHC σ_{xy} as follows. The number of electrons with each spin direction is given in Table III. In Ni, the d band of the majority spins ($\downarrow$) is almost filled, and therefore $\sigma_{xy}^{\downarrow}$ is rather small. On the other hand, $n_{d\uparrow} \simeq 4.15$, and thus $\sigma_{xy}^{\uparrow}$ is rather large and positive. Then, the AHC in Ni is mainly caused by minority spins ($\uparrow$), and therefore $\sigma_{xy} \simeq -2\sigma_{xy}^{\uparrow} < 0$. In Co, the d band of majority spins is almost filled as in Ni, and therefore $\sigma_{xy}^{\downarrow}(>0)$ is rather small. However, $\sigma_{xy}^{\uparrow}$ is smaller, because $n_{d\uparrow} \simeq 3.1 (n_{\uparrow} \simeq 3.7)$, around where the sign of σ_{xy}^{S} changes. After all, majority spins mainly contribute to σ_{xy} in Co, and therefore $\sigma_{xy} \simeq 2\sigma_{xy}^{\downarrow} > 0$.

TABLE III. Number of the minority spins $n_{\uparrow}$ and majority spins $n_{\downarrow}$ in $3d$ ferromagnetic transition metals (Ref. 43). In parentheses, number of d electrons of each spin direction is shown.

	Fe	Co	Ni
$n_{\uparrow}(n_{d\uparrow})$	2.95(2.34)	3.67(3.06)	4.66(4.15)
$n_{\downarrow}(n_{d\downarrow})$	5.05(4.59)	5.32(4.82)	5.33(4.82)

We also calculate the SHC in the ferromagnetic phase of Fe, Co, and Ni. From the results for the SHC and those for the AHC, we obtain σ_{xy}^{σ} using Eqs. (23) and (24) and plot the data of $2\sigma_{xy}^{\sigma}$ at $2n_{\sigma}$ in Fig. 3 for Fe, Co, and Ni.[44] The data for Fe are obtained with the tight-binding parameter set that is described in the Appendix. It can indeed be seen that those data are consistent with the trend of σ_{xy}^{S} as a function of n, corroborating the above explanation.

V. SUMMARY AND DISCUSSION

We calculated the AHC in ferromagnetic $3d$ transition metals using realistic tight-binding models and resorting to the linear-response theory, assuming the intrinsic mechanism. Our results are semiquantitatively agree with previous experimental and theoretical results, supporting the validity of the intrinsic mechanism of the AHE in ferromagnetic $3d$ transition metals. The present theory proceeds in perfect parallelism with the one for the SHE in $4d$ and $5d$ transition metals we developed previously.[30] Therefore, the origin of large anomalous Hall effect must also be ascribable to the effective Aharonov-Bohm flux generated by combination of orbitally dependent electron transfers and spin-orbit interaction, as in the case with the SHE in $4d$ and $5d$ transition metals.[30]

Using the parallelism between the AHE and the SHE, we can explain the magnitude and sign of the AHC in $3d$ transition metals. The dependence of the Hall conductivity of each spin component σ_{xy}^{σ} on the electron number was successfully explained in Ref. 31. Sign of σ_{xy}^{σ} is determined by Hund's rule coupling $\langle \ell_z s_z \rangle/\hbar^2$, which is proportional to spin-orbit interaction λ, and is negative for light transition elements and positive for heavy ones. Generally, spin-orbit interaction λ is large in heavier elements. In noble metals, spin-orbit interaction may be large, but electrons near the Fermi surface are mainly s electrons, for which spin-orbit interaction is insignificant. Hall conductivity σ_{xy}^{σ} is therefore

TABLE IV. Anomalous Hall conductivity σ_{xy} in 3*d* ferromagnetic transition metals.

σ_{xy} $[(\Omega\ \mathrm{cm})^{-1}]$	Fe	Co	Ni
NRL-TB	247	341	−1087
Two center, ortho.	805	404	−888
Experiment	1032[a]	205[b]	−646[c]

[a]Reference 39.
[b]Reference 40.
[c]Reference 41.

negative in light transition metals, and positive in heavy transition metals. The absolute magnitude of σ_{xy}^{σ} is generally larger in heavier elements but is small in noble metals (Cu, Ag, and Au). From this trend of σ_{xy}^{σ} and the number of each spin component in ferromagnetic transition metals, we were able to explain the sign (and the magnitude) of the AHC in the 3*d* transition ferromagnets.

We have found that the AHC (due to the intrinsic mechanism) is insensitive to impurity concentration in the clean limit, but depends on it, $\sigma_{xy} \propto \gamma^{-2}$, as the system becomes dirty. In the clean limit, the AHC can be expressed with integral of Berry curvature over occupied states. However, as impurity concentration increases, the AHC cannot be expressed only with the Berry curvature term. Indeed, the AHC is well approximated not by the Berry curvature term, but by the Fermi surface term, in a wider range of impurity concentration. The same conclusion was also obtained for the SHC.[30] This would be an important point when discussing the crossover behavior of the AHE from the clean limit to dirty limit.

Indeed, Miyasato *et al.*[42] measured the AHC in various itinerant ferromagnets, and observed crossover behavior of the AHC as a function of conductivity σ_{xx}, which they claimed is explained by a theory developed by Onoda *et al.*[45] They found that $\sigma_{xy} \sim \sigma_{xx}^{1.6}$ in the dirty region in harmony with what was found in Ref. 45. A few comments are in order here. First, in the experiments, electron number density differs in samples of different compositions. The AHC generally depends upon electron number density. Then, in discussing the dependence of the AHC on resistivity, one must be careful about the change in electron number density. Second, relation $\sigma_{xy} \sim \sigma_{xx}^{1.6}$ was observed in a very dirty region, where resistivity ρ is much larger than 100 $\mu\Omega$ cm.[42] In that region, electronic states cannot be correctly described by a simple theory such as the *T*-matrix one used in Ref. 45. In the present theory, we confine ourselves to the cases where $\gamma \ll W$, W being the typical band width, and $\rho \lesssim 100$ $\mu\Omega$ cm. Third, the AHE was analyzed using the Rashba model in Ref. 45. The Rashba model may be appropriate for some materials but it is quite a special model in that it assumes spatial asymmetry. It may be unlikely that one can explain universal behavior of the AHE on the basis of such a special model. It should be noted that there is also a report that $\sigma_{xy} \propto \sigma_{xx}^{2}$ holds.[46]

We have seen that the quantitative agreement between experimental and theoretical results for the AHC has not yet been obtained. While careful analyses of measurements are highly desired, there are also a lot of possible improvement of calculations. It is possible that a more sophisticated first-principles calculation and consideration of the electron correlation effect would give quantitatively different results of the AHC. There are still a lot of challenges on both experimental and theoretical sides.

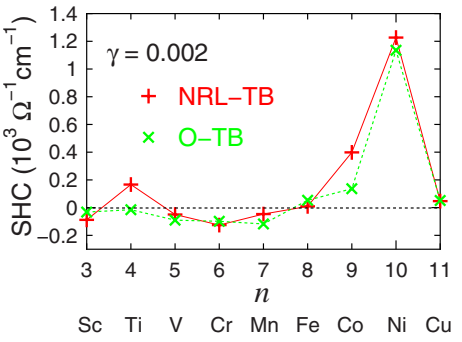

FIG. 4. (Color online) Spin-Hall conductivity $\sigma_{xy}^{S}(\times|e|/\hbar)$ of 3*d* transition metals calculated with the use of NRL-TB and O-TB models. Damping rate γ is γ=0.002 Ry.

ACKNOWLEDGMENTS

This work was partially supported by Grant-in-Aid for Science Research on Priority Area, Ministry of Education, Science, and Culture of Japan. We are grateful to T. Tanaka for much help in numerical calculations.

APPENDIX: COMPARISON WITH RESULTS OBTAINED WITH OTHER TIGHT-BINDING MODELS

NRL-TB model reproduces the results of first-principles calculation with high precision. The typical error is estimated to be 0.002–0.004 Ry.[47] The true strength of the NRL-TB model consists in its transferability.[48] The parameter set given for an element can be used to describe the band structure with various values of the lattice constant and also the band structure with different crystal structures. This is certainly a merit but it also means that the NRL-TB model is not necessarily the best model for the band structure with a particular crystal structure and a lattice constant, e.g., the band structure at room temperature and ambient pressure. It is not obvious whether the fine details near the Fermi energy, which make dominant contributions to the AHC, are described very precisely with the NRL-TB model. Therefore, we calculate the AHC and SHC of 3*d* transition metals using other tight-binding models that can describe the band structures of those metals quantitatively well, and compare results with those obtained with the NRL-TB model.

We use the tight-binding parameters given in Ref. 43. Actually, four different parameter sets are given for an element there: Slater-Koster three-center parameters with orthogonal and nonorthogonal orbitals, and Slater-Koster two-center parameters with orthogonal and nonorthogonal orbitals. In this work, we use the latter two parameter sets (two-center parameters). Electron transfer integrals up to the

second- or the third-neighbor sites are considered. As there are more parameters with nonorthogonal bases than with orthogonal bases, the fitting of the band structure is generally better with nonorthogonal bases. In the following, we abbreviate the tight-binding model with two center and orthogonal scheme as the O-TB model, and the tight-binding model with two-center and nonorthogonal scheme as the NO-TB model.

In Table IV, we show the results for the AHC of 3*d* transient ferromagnetic metals obtained with the NRL-TB model and the O-TB model. It can be seen that, for Co and Ni, the results obtained with the two models agree satisfactorily, but there is a significant difference for Fe.

Figure 4 shows the SHC of 3*d* transition metals obtained with the NRL-TB and the O-TB models. The paramagnetic state is assumed for all the elements. The general trend is consistently obtained with both models but the difference between the results is significant for Ti and Co. In Ti, particularly, sign of σ_{xy}^{S} is found to change. It is difficult to clarify the reason for the difference between results obtained with the two models, but it should be noted that there are more than one equilibrium solid phases in Ti, Co, and Fe,[49] where results of the AHC or SHC significantly depend on used models. For example, at room temperature and ambient pressure, Ti is in a hcp structure, and at high pressure ($\gtrsim$2 GPa) and room temperature, it transforms into another hexagonal phase. At ambient pressure and high temperatures ($>$1155 K), Ti is in a bcc structure. This may be relevant for the difference in results obtained with the two models.

[1] R. Karplus and J. M. Luttinger, Phys. Rev. **95**, 1154 (1954).
[2] J. Smit, Physica (Amsterdam) **24**, 39 (1958).
[3] L. Berger, Phys. Rev. B **2**, 4559 (1970).
[4] H. Kontani and K. Yamada, J. Phys. Soc. Jpn. **63**, 2627 (1994).
[5] H. Kontani and K. Yamada, J. Phys. Soc. Jpn. **66**, 2252 (1997).
[6] M. Miyazawa, H. Kontani, and K. Yamada, J. Phys. Soc. Jpn. **68**, 1625 (1999).
[7] Z. Fang, N. Nagaosa, K. S. Takahashi, A. Asamitsu, R. Mathieu, T. Ogasawara, H. Yamada, M. Kawasaki, Y. Tokura, and K. Terakura, Science **302**, 92 (2003).
[8] Y. Yao, L. Kleinman, A. H. MacDonald, J. Sinova, T. Jungwirth, D. S. Wang, E. Wang, and Q. Niu, Phys. Rev. Lett. **92**, 037204 (2004).
[9] X. Wang, J. R. Yates, I. Souza, and D. Vanderbilt, Phys. Rev. B **74**, 195118 (2006).
[10] X. Wang, D. Vanderbilt, J. R. Yates, and I. Souza, Phys. Rev. B **76**, 195109 (2007).
[11] M. I. Dyakonov and V. I. Perel, JETP Lett. **13**, 467 (1971).
[12] J. E. Hirsch, Phys. Rev. Lett. **83**, 1834 (1999).
[13] G. Sundaram and Q. Niu, Phys. Rev. B **59**, 14915 (1999).
[14] S. Onoda and N. Nagaosa, J. Phys. Soc. Jpn. **71**, 19 (2002).
[15] P. Streda, J. Phys. C **15**, L717 (1982).
[16] H. Kontani, T. Tanaka, and K. Yamada, Phys. Rev. **75**, 184416 (2007).
[17] M. J. Mehl and D. A. Papaconstantopoulos, Phys. Rev. B **54**, 4519 (1996).
[18] D. A. Papaconstantopoulos and M. J. Mehl, J. Phys.: Condens. Matter **15**, R413 (2003).
[19] In Refs. 9 and 10, they construct Wannier functions from the results of first-principles calculations and then describe the electronic states with tight-binding models. They then were able to calculate AHC using a fine mesh of the Brillouin zone.
[20] Y. K. Kato, R. C. Meyer, A. C. Gossard, and D. D. Awschalom, Science **306**, 1910 (2004).
[21] J. Wunderlich, B. Kaestner, J. Sinova, and T. Jungwirth, Phys. Rev. Lett. **94**, 047204 (2005).
[22] S. O. Valenzuela and M. Tinkham, Nature (London) **442**, 176 (2006).
[23] E. Saitoh, M. Ueda, H. Miyajima, and G. Tatara, Appl. Phys. Lett. **88**, 182509 (2006).
[24] T. Kimura, Y. Otani, T. Sato, S. Takahashi, and S. Maekawa, Phys. Rev. Lett. **98**, 156601 (2007).
[25] S. Murakami, N. Nagaosa, and S. C. Zhang, Science **301**, 1348 (2003).
[26] J. Sinova, D. Culcer, Q. Niu, N. A. Sinitsyn, T. Jungwirth, and A. H. MacDonald, Phys. Rev. Lett. **92**, 126603 (2004).
[27] H. Kontani, T. Tanaka, D. S. Hirashima, K. Yamada, and J. Inoue, Phys. Rev. Lett. **100**, 096601 (2008).
[28] G. Y. Guo, S. Murakami, T.-W. Chen, and N. Nagaosa, Phys. Rev. Lett. **100**, 096401 (2008).
[29] H. Kontani, M. Naito, D. S. Hirashima, K. Yamada, and J. Inoue, J. Phys. Soc. Jpn. **76**, 103702 (2007).
[30] T. Tanaka, H. Kontani, M. Naito, T. Naito, D. S. Hirashima, K. Yamada, and J. Inoue, Phys. Rev. B **77**, 165117 (2008).
[31] H. Kontani, T. Tanaka, D. S. Hirashima, K. Yamada, and J. Inoue, Phys. Rev. Lett. **102**, 016601 (2009).
[32] M. Morota, K. Ohnishi, T. Kimura, and Y. Otani, J. Appl. Phys. **105**, 07C712 (2009).
[33] F. Herman and S. Skillman, *Atomic Structure Calculations* (Prentice-Hall, Englewood Cliffs, New Jersey, 1963).
[34] For 4*s* and 4*p* orbitals, the damping rate can be significantly different. However, contributions from those electrons are much smaller than those from *d* electrons and the precise values of damping rate for 4*s* and 4*p* electrons do not matter.
[35] This relation also holds at finite temperatures.
[36] For example, N. I. Kulikov and E. T. Kulatov, J. Phys. F: Met. Phys. **12**, 2267 (1982).
[37] For example, C. S. Wang and J. Callaway, Phys. Rev. B **9**, 4897 (1974).
[38] As $\gamma \to 0$, resistivity ρ is proportional to γ, but ρ may not necessarily be proportional to γ as γ becomes large. Therefore, $\sigma_{xy} \propto \rho^{-2}$ may not necessarily be observed.
[39] P. Dheer, Phys. Rev. **156**, 637 (1967).
[40] J. Kötzler and W. Gil, Phys. Rev. B **72**, 060412(R) (2005).
[41] J. M. Lavine, Phys. Rev. **123**, 1273 (1961).
[42] T. Miyasato, N. Abe, T. Fujii, A. Asamitsu, S. Onoda, Y. Onose, N. Nagaosa, and Y. Tokura, Phys. Rev. Lett. **99**, 086602 (2007). The values of the AHC read from Fig. 1 are approximately: 1930 for an Fe crystal, 900 for an Fe film, 460 for a Co film, and 460 for a Ni film, in units of $(\Omega\ \mathrm{cm})^{-1}$.
[43] D. A. Papaconstantopoulos, *Handbook of the Band Structure of Elemental Solids* (Plenum Press, New York, 1986).

[44] In Fe, $\sigma_{xy}^{\uparrow}<0$, $\sigma_{xy}^{\downarrow}>0$, and $\sigma_{xy}\simeq-2(\sigma_{xy}^{\uparrow}-\sigma_{xy}^{\downarrow})>0$. In contrast to the cases with Co and Ni, $|\sigma_{xy}^{\uparrow}|\simeq|\sigma_{xy}^{\downarrow}|$, and both components positively contribute to σ_{xy}.

[45] S. Onoda, N. Sugimoto, and N. Nagaosa, Phys. Rev. Lett. **97**, 126602 (2006).

[46] D. Satoh, K. Okamoto, and T. Katsufuji, Phys. Rev. B **77**, 121201(R) (2008).

[47] D. A. Papaconstantopoulos and I. Mazin (private communication).

[48] N. C. Bacalis, D. A. Papaconstantopoulos, M. J. Mehl, and M. Lach-Hab, Physica B **296**, 125 (2001).

[49] D. A. Young, *Phase Diagram of the Elements* (University of California Press, Berkeley, 1991).